A Software Platform for the Comparative Analysis of Electroanatomic and Imaging Data including Conduction Velocity Mapping

Chris D. Cantwell[1], Caroline H. Roney[2], Rheeda L. Ali[2], Norman A. Qureshi[1], Phang Boon Lim[1] and Nicholas S. Peters[1]

Abstract— **Electroanatomic mapping systems collect increasingly large quantities of spatially-distributed electrical data which may be potentially further scrutinized post-operatively to expose mechanistic properties which sustain and perpetuate atrial fibrillation. We describe a modular software platform, developed to post-process and rapidly analyse data exported from electroanatomic mapping systems using a range of existing and novel algorithms. Imaging data highlighting regions of scar can also be overlaid for comparison. In particular, we describe the conduction velocity (CV) mapping algorithm used to highlight wavefront behaviour. CV was found to be particularly sensitive to the spatial distribution of the triangulation points and corresponding activation times. A set of geometric conditions were devised for selecting suitable triangulations of the electrogram set for generating CV maps.**

I. INTRODUCTION

Cardiac arrhythmias, such as atrial fibrillation (AF), are a leading cause of mortality in the UK [1], leading to reduced quality of life and increased risk of complications, such as stroke. However, the mechanisms which initiate and perpetuate them are poorly understood. Catheter ablation is typically used to treat the condition by modifying the endocardial substrate using focused radio-frequency energy, delivered via a catheter, to modify the electrical pathways in the myocardium. Current 3D electroanatomic mapping systems are now commonly used during these procedures and can rapidly collect large quantities of spatially-distributed electrical data which is processed in real-time to visually display summary statistics such as local activation time, peak-to-peak voltage or a complex fractionation score. Automatically summarising and analysing electrogram data is therefore becoming increasingly essential for clinical interpretation, diagnosis and treatment planning.

These rich electrical datasets, along with imaging data such as late-gadolinium enhanced magnetic resonance imaging (LGE-MRI), may be potentially further scrutinized post-operatively using novel algorithms to increase our understanding of the underlying processes occuring in AF and expose mechanistic properties which sustain and perpetuate the condition. However, implementing and testing new analysis algorithms and incorporating co-localised imaging data is challenging with current electroanatomic mapping systems. Furthermore, these systems include limited scope for analyses which depend on the spatial arrangement and relative locality of signals on the endocardial surface.

Conduction velocity is an example of a spatially dependent statistic and is of particular interest to cardiac electrophysiologists as a surrogate measure for fibrosis and poor conduction. A number of existing approaches have been considered for processing electrophysiological data and evaluating velocity information, for example polynomial surface-fitting algorithms [3], [4], finite-difference techniques [5], [6] and triangulation [7]. However, these techniques either require regularly spaced high-density data points, can only be applied at a regional level (coarse resolution), or are manual in nature. Clinical data is not regularly spaced and the volume of data makes manual algorithms impractical.

We describe an open-source modular software platform designed to support post-operative analysis of electrical and imaging datasets and facilitate the development of new high-density electrogram analysis algorithms. An overview of the platform architecture is given and we present details of an automated conduction velocity mapping algorithm developed within the framework.

II. PLATFORM OVERVIEW

The platform enables the post-processing of unipolar or bipolar electroanatomic datasets, exported from the Ensite Velocity system (St Jude Medical, Inc) [2], and enables the rapid analysis of the electrogram signals using a range of existing and novel algorithms. The chamber surface model is constructed during the mapping procedure and is exported from the mapping system as an endocardial surface triangulation. Multiple maps recorded during the procedure may be loaded concurrently for comparison of data recorded under different protocols. Additionally, pre-operative imaging data indicating regions of fibrosis may be simultenously loaded with the externally registered electroanatomical data and overlaid for comparison.

The graphical interface for the platform, shown in Fig. 1, is implemented in C++ using the Qt [8] library for the user interface and the VTK [9] libraries for the visualisation pipeline. The central component of the platform is the anatomical display showing the chamber geometry with a computed summary statistic, such as local activation time or peak-to-peak voltage amplitude, projected on the surface. Statistics are computed at the electrogram points and interpolated on the surface (up to a user-defined maximum distance) using a distance-weighted average of nearby points

[1]National Heart and Lung Institute, Imperial College London, South Kensington Campus, London SW7 2AZ, UK {c.cantwell, n.qureshi, p.b.lim, n.peters} at imperial.ac.uk

[2]Department of Bioengineering, Imperial College London, South Kensington Campus, London SW7 2AZ, UK {caroline.roney10, rheeda.ali07} at imperial.ac.uk

978-1-4244-7929-0/14/$26.00 ©2014 IEEE

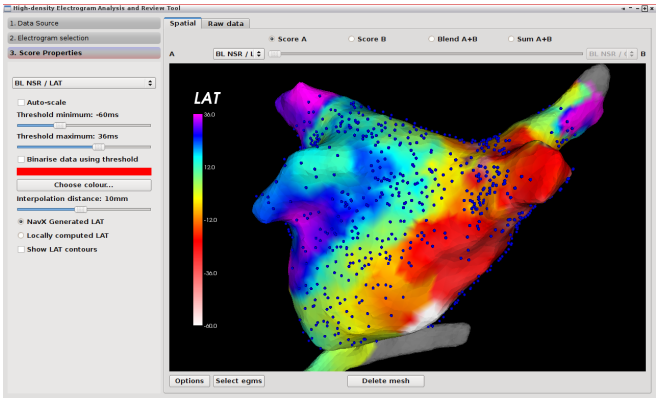

Fig. 1. Graphical user interface for the analysis platform showing visualisation of the chamber with local activation time (LAT) projected on the surface. Electrogram recording points are indicated with blue dots.

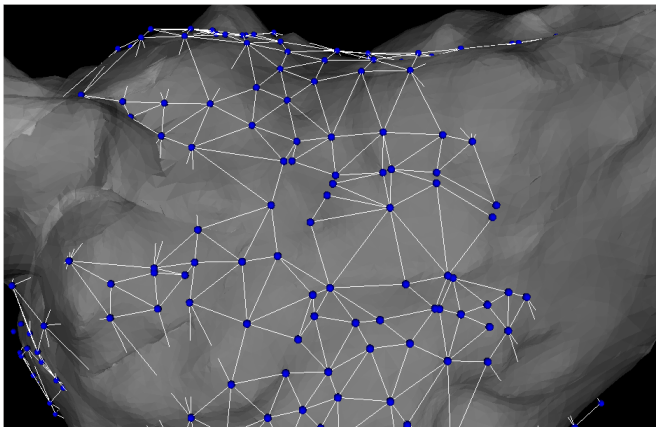

Fig. 2. Electrogram points (blue circles) are triangulated using a modified Delaunay algorithm. Triangles which do not satisfy the criteria are rejected.

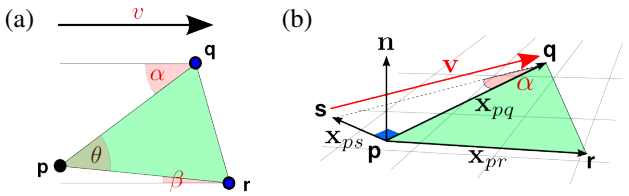

Fig. 3. Diagram illustrating (a) the conduction speed calculation and (b) velocity vector calculation, ensuring the velocity vector is coplanar with the triangle vertices p, q and r.

[10]. The geometry may be rotated and magnified by the user and areas of the chamber surface may be selected and removed from the analysis to focus on a region of interest. The displayed statistic is chosen from the drop-down list, and the panel on the left of the user interface allows for customisation of the algorithms used. Additional options enable the user to customise the rendered image, such as removing the electrogram points, colour bar and chamber surface, to aid analysis.

When processing clinically recorded data it is important to filter out those recordings which are of insufficient quality to analyse confidently. This may be due to poor contact with the myocardium, interference due to far-field effects or electrical noise in the recorded signal. Individual electrograms may be examined in both the time domain and the frequency domain, and undesirable recordings may be disabled and subsequently excluded from further use in analysis. The numerical values of the summary statistics for each electrogram are also available for direct quantative comparison.

A range of existing algorithms are implemented in the platform, including local activation time (LAT), maximum peak-to-peak voltage, fractionation scores (average cycle length, shortest cycle length) [11], [12], continuous atrial activity [13], dominant frequency, FFT ratio [14] and organisational index [15]. A number of novel algorithms including conduction velocity and time-averaged peak-to-peak deflection voltage have also been implemented. Spatial comparison of scores may be achieved through blending or through threshold binarisation of the scores. In the latter, regions in which the value of a statistic falls within a restricted range are assigned a single colour, while those outside the range are not displayed. The resulting maps may be overlaid and regions of overlap identified and quantified in terms of area of coverage.

III. CONDUCTION VELOCITY MAPPING

We now describe the automated conduction velocity algorithm implemented in the platform. To compute localised conduction velocity requires activation times at a minimum of three non-colinear points in order to establish both speed and direction of conduction. We therefore apply Delaunay triangulation [16] to the electrode point cloud to generate a set of non-overlapping triangles, thereby maximising coverage while minimising computational cost. Conduction velocity magnitude and direction is sensitive to measurement errors. We therefore impose the following criteria before accepting a triangle:

- Distances between vertices are $\geq 3mm$. This excludes particularly small triangles where measurement error in the location is relatively high.
- Local activation times have been successfully computed for all points in the triangle.
- Local activation time differences along at least two sides of the triangle are $\geq 3ms$. Conduction velocity will be increasingly susceptible to LAT measurement error when time differences are small. The constraint still allows for activation normal to one side of the triangle in which two vertices activate simulteneously.
- Ratio of circumcircle area to triangle area is < 10. This prevents the inclusion of particularly elongated triangles where measurement error may result in a distortion of the direction calculation.

A triangulation of electrode locations over the posterior wall and roof of example clinical data is shown in Fig. 2. One limitation of the algorithm is that densly packed areas of electrogram recordings may in fact result in no valid triangles due to the minimum distance constraints coupled with the Delaunay criterion. However, we have not observed this to be a significant problem in practice.

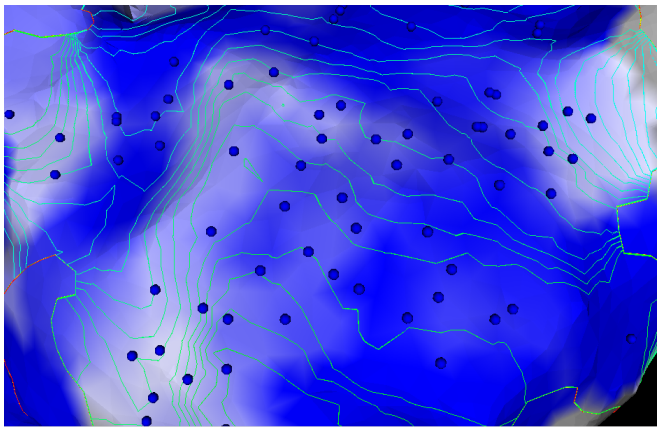

Fig. 4. Map of conduction speed with contours of local activation time. White indicates areas of low conduction speed, while blue indicated high conduction speed. Measurement points are indicated with blue circles.

In computing the conduction speed, we initially follow the method described in Kojodjojo *et al* [7] and which is illustrated in Fig. 3(a). The notation used is as follows. A vector from point p to point q is denoted as $\mathbf{x}_{pq}$, $||\mathbf{x}_{pq}||$ is therefore its corresponding length, and t_{pq} is the difference in local activation times between the two points. The angle θ can be computed direcly using the cosine rule as

$$\theta = \arccos\left(\frac{||\mathbf{x}_{pq}||^2 + ||\mathbf{x}_{pr}||^2 - ||\mathbf{x}_{qr}||^2}{2||\mathbf{x}_{pq}||\,||\mathbf{x}_{pr}||}\right),$$

and we can then express three relationships between the three unknown quantities — speed v and angles α and β — in terms of θ and the known distances and local activation times between the three vertices of the triangle,

$$\cos\beta = \cos(\theta - \alpha), \tag{1}$$

$$v = \frac{||\mathbf{x}_{pq}||\cos\alpha}{t_{pq}}, \tag{2}$$

$$v = \frac{||\mathbf{x}_{pr}||\cos\beta}{t_{pr}}. \tag{3}$$

The angle α can be computed as

$$\Rightarrow \tan\alpha = \frac{\frac{t_{pr}||\mathbf{x}_{pq}||}{t_{pq}||\mathbf{x}_{pr}||} - \cos\theta}{\sin\theta},$$

and β and v follow directly from Equations (1)-(3). The spatial distribution of conduction speed is presented visually on the anatomical rendering of the patient's left atrial chamber geometry in Fig. 4. Regions of low conduction speed (indicated in white) are seen to correspond to bunching of the local activation time contours as expected. Conduction speeds for the example data shown are in the physiological range of 0.07-1.30m/s [17], with an average conduction velocity of 0.61m/s.

We now extend the technique to compute the velocity vector within a triangle on the three-dimensional surface. This vector must be coplanar with the three vertices of the triangle and we therefore begin by computing the normal to the triangle,

$$\hat{\boldsymbol{n}} = \frac{\mathbf{x}_{pr} \times \mathbf{x}_{pq}}{||\mathbf{x}_{pr} \times \mathbf{x}_{pq}||}$$

Referring to Fig. 3 we now compute the extrusion from point p, perpendicular to $\mathbf{x}_{pq}$, and thus the intersection with the velocity vector, denoted s,

$$\mathbf{x}_{ps} = (\hat{\mathbf{n}} \times \mathbf{x}_{pq})\tan\alpha,$$

and finally the required velocity vector

$$\mathbf{v} = \mathbf{x}_{pq} - \mathbf{x}_{ps}.$$

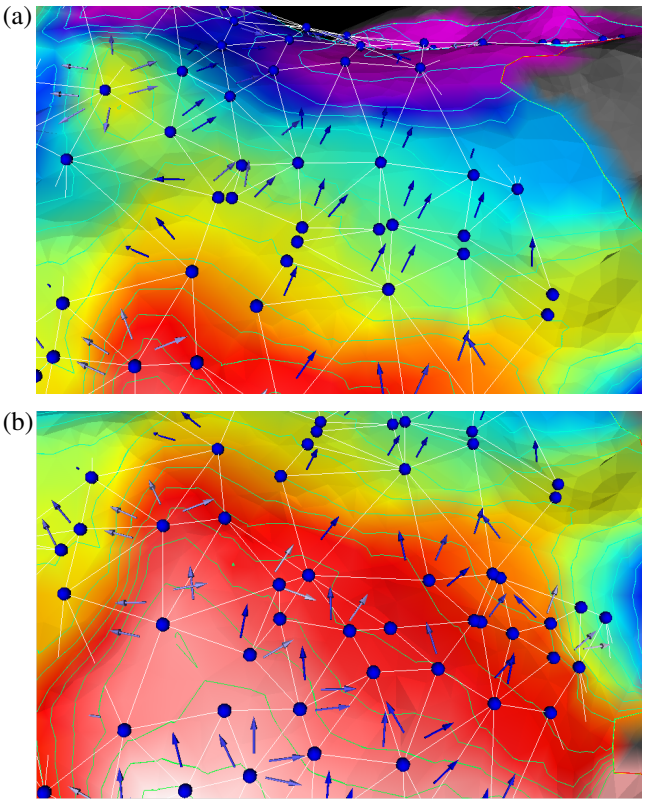

Fig. 5. Conduction velocity vector field on (a) the left atrial roof and (b) the posterior wall, overlaid on the local activation time map (white: early activation, purple: late activation) with contours.

Fig. 5 shows the local activation time map for the roof and posterior wall of the left atrium with the velocity vector field superimposed. The wavefront propagation over the roof is seen to be unidirectional while the posterior wall is less organised. Velocity vector directions are predominantly perpendicular to the contours of LAT. In particular, vectors in areas of slow conduction appear to better capture wavefront direction due to the greater difference in activation times between vertices of the triangle.

IV. DISCUSSION

The described open-source software platform[1] provides access to a range of electroanatomic analysis algorithms which can be applied to clinically acquired mapping data.

[1]The software and source code is available upon request.

The graphical interface developed allows for the rapid analysis and visualisation of spatially distributed summary statistics. In particular, we have implemented an automated conduction velocity mapping algorithm and demonstrated its effectiveness at mapping the direction of activation wavefronts in real clinical data. While this algorithm is qualitatively shown to be accurate with respect to the contours of local activation in the context of paced rhythms, measurements on experimental data and verified with a second modality would allow the sensitivity of the algorithm to measurement errors to be quantified.

To conclude, we illustrate the potential use of the platform for analysing data. Fig. 6(a) shows a map of maximum peak-to-peak voltage (maximum deflection amplitude) with the range of interest restricted to 0-1.5mV. Areas in purple exceed a peak-to-peak voltage of 1.5mV. The pulmonary veins and mitral valve have been excluded to facilitate comparison of the main chamber walls. Fig. 6(b) shows a comparison of low peak-to-peak voltage and slow conduction speed. The binarised image highlights in red regions where conduction velocity is below 0.5m/s, while peak-to-peak voltages below 1.5mV are highlighted in green. Areas in brown show the overlap of the two subsets. The area of each individual score, as well as the area of overlap is calculated in terms of mm^2. In this particular example 70% of the area of slow conduction velocity overlaps with regions of low peak-to-peak voltage. Such analyses can support hypothesis testing and maximise the use of clinically acquired data.

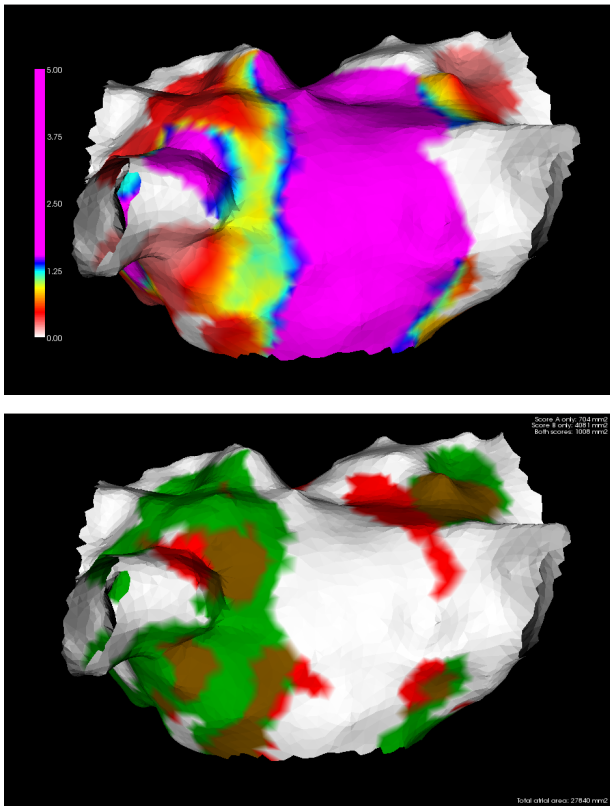

Fig. 6. (a) Peak to peak voltage, with colour scale restricted to the range 0.0-1.5mV. (b) Binarised comparison of slow conduction velocity only (red), low peak-to-peak voltage only (green) and both (brown). Areas for these three subsets are computed in the upper-right corner of the display.

ACKNOWLEDGMENT

This work was supported by the British Heart Foundation (BHF), grants FS/11/22/28745 & RG/10/11/28457, EPSRC grant EP/K038788/1 and the ElectroCardioMaths Programme of the Imperial BHF Centre of Research Excellence and NIHR Imperial Biomedical Research Centre.

REFERENCES

[1] A.G. Kleber and Y. Rudy, *Basic mechanisms of cardiac impulse propagation and associated arrhythmias*. Physiological reviews, 84(2):431, 2004.

[2] C. Eitel, G. Hindricks, N. Dagres, P. Sommer, C. Piorkowski, *EnSite Velocity cardiac mapping system: a new platform for 3D mapping of cardiac arrhythmias.*, Informa Healthcare London, 2010.

[3] P. V. Bayly, B. H. KenKnight, J. M. Rogers, R. E. Hillsley, R. E. Ideker, W. M. Smith. *Estimation of conduction velocity vector fields from epicardial mapping data.* IEEE transactions on bio-medical engineering, 45(5):563–71, 1998.

[4] A. R. Barnette, P. V. Bayly, S. Zhang, G. P. Walcott, R. E. Ideker, W. M. Smith, *Estimation of 3-D conduction velocity vector fields from cardiac mapping data*, IEEE transactions on bio-medical engineering, 47(8):1027–35.

[5] G. Salama, A. Kanai, and I. R. Efimov, *Subthreshold stimulation of Purkinje fibers interrupts ventricular tachycardia in intact hearts. Experimental study with voltage-sensitive dyes and imaging techniques*, Circulation Research, 74(4):604–619, 1994.

[6] J. I. Laughner, F. S. Ng, M. S. Sulkin, R. M. Arthur, I. R. Efimov (2012). *Processing and analysis of cardiac optical mapping data obtained with potentiometric dyes*, American journal of physiology. Heart and circulatory physiology, 303(7):H753–65, 2012.

[7] P. Kojodjojo, P. Kanagaratnam, V. Markides, D. W. Davies, and N. Peters, *Age-related changes in Human Left and Right Atrial Conduction*. J Cardiovasc Electrophysiol, 17(2), 2006.

[8] Nokia Corporation, *Qt reference documentation.* http://doc.qt.nokia.com/4.8 (2014). Accessed 13 Mar 2014.

[9] *VTK*, http://www.vtk.org (2014). Accessed 13 Mar 2014.

[10] D. Shepard, *A two-dimensional interpolation function for irregularly-spaced data*. Proceedings of the 1968 ACM National Conference. pp. 517524, 1968.

[11] R. J. Hunter, I. Diab, G. Thomas, E. Duncan, D. Abrams, M. Dhinoja, S. Sporton, M. J. Earley, R. J. Schilling, *Validation of a classification system to grade fractionation in atrial fibrillation and correlation with automated detection systems*, Europace. 11(12):1587-96, 2009.

[12] J. Wu, H. Estner, A. Luik, E. Ucer, T. Reents, A. Pflaumer, B. Zrenner, G. Hessling, I. Deisenhofer, *Automatic 3D mapping of complex fractionated atrial electrograms (CFAE) in patients with paroxysmal and persistent atrial fibrillation*, J Cardiovasc Electrophysiol. 19(9):897-903, 2008.

[13] Y. Takahashi, M.D. O'Neill, M. Hocini, R. Dubois, S. Matsuo, S. Knecht, S. Mahapatra, K. T. Lim, P. Jas, A. Jonsson, F. Sacher, P. Sanders, T. Rostock, P. Bordachar, J. Clémenty, G. J. Klein, M. Hassaguerre, *Characterization of electrograms associated with termination of chronic atrial fibrillation by catheter ablation*, J Am Coll Cardiol. 51(10):1003-10, 2008.

[14] L. Saghy, D. J. Callans, F. Garcia, D. Lin, F. E. Marchlinski, M. Riley, S. Dixit, W. S. Tzou, H. M. Haqqani, R. Pap, S. Kim, E. P. Gerstenfeld, *Is there a relationship between complex fractionated atrial electrograms recorded during atrial fibrillation and sinus rhythm fractionation?*, Heart Rhythm. 9(2):181-8, 2012.

[15] T.H. Everett, J. R. Moorman, L. C. Kok, J. G. Akar, D. E. Haines, *Assessment of global atrial fibrillation organization to optimize timing of atrial defibrillation*, Circulation. 103(23):2857-61, 2001.

[16] B. Delaunay, *Sur la sphère vide. A la mémoire de Georges Vorono*, Bulletin de l'Académie des Sciences de l'URSS. Classe des sciences mathématiques et na, 6:793–800, 1934.

[17] P. Kanagaratnam, S. Rothery, P. Patel, N.J. Severs, N.S. Peters. *Relative expression of immunolocalized connexins 40 and 43 correlates with human atrial conduction properties*, J Am Coll Cardiol. 39(1), pp. 116-23, 2002.